

NASA TECHNICAL NOTE



NASA TN D-3154

NASA TN D-3154

LOAN COPY: RE  
AFWL (WLI  
KIRTLAND AFB,



EXPERIMENTAL AND THEORETICAL EVALUATION  
OF A PASSIVE COMMUNICATIONS SATELLITE  
(ECHO II)

by

*A. Kampinsky*  
*Goddard Space Flight Center*

and

*R. K. Ritt*  
*Conduction Corporation*



TECH LIBRARY KAFB, NM



0079889

NASA TN D-3154

EXPERIMENTAL AND THEORETICAL EVALUATION  
OF A PASSIVE COMMUNICATIONS SATELLITE

(ECHO II)

By A. Kampinsky

Goddard Space Flight Center  
Greenbelt, Md.

and

R. K. Ritt

Conduction Corporation  
Ann Arbor, Mich.

NATIONAL AERONAUTICS AND SPACE ADMINISTRATION

---

For sale by the Clearinghouse for Federal Scientific and Technical Information  
Springfield, Virginia 22151 - Price \$2.00

## ABSTRACT

A three-part program has been completed which assessed the performance of a passive satellite communications system—the thin-wall-stressed-skin balloon—Echo II. The first program phase involved evaluating the backscatter characteristics of a small segment of this large spherical (or lenticular) structure in terms of inherent distortions which can be related to physical construction or dynamic distortions in orbit. The next program phase, prior to flight, evaluated full-size Echo II spheres to demonstrate the relationships between the skin-stress-scintillation level and backscatter qualities for actual balloons. The final, or flight program, phase included twenty operational and experimental radar systems and provided both backscatter data and communications data in real time for the Echo balloon from a few hours after injection (25 January 1964) into orbit until December 1964. A basic measurements program has evolved which can, by measurement of judiciously defined spherical segments, economically and accurately measure the parameters of response on segments of reasonable dimensions. Valid extrapolations of electromagnetic responses for passive structures having dimensions of from one to two orders of magnitude or larger can be made; thus, large balloons need not be inflated prior to flight to determine quality as communication devices.

## CONTENTS

Abstract . . . . .	ii
Foreword . . . . .	v
INTRODUCTION . . . . .	1
SMALL SEGMENT MEASUREMENTS (PHASE I) . . . . .	2
MATHEMATICAL MODEL OF THE BALLOON . . . . .	6
FULL SCALE BALLOON (PHASE II) . . . . .	6
PRELUDE TO THE ORBITAL BALLOON (PHASE III) . . . . .	11
ECHO II ORBITAL FLIGHT RADAR DATA AND ANALYSIS . . . . .	15
EFFECTIVENESS AS A COMMUNICATION SATELLITE . . . . .	18
Radar Cross Section Statistics . . . . .	21
Fading Rate . . . . .	22
Signal Modulation by the Balloon . . . . .	22
COMMUNICATIONS EXPERIMENT . . . . .	24
ADDITIONAL DATA . . . . .	25
References . . . . .	27
Appendix A—Equations of Membrane Forces . . . . .	29
Appendix B—Mathematical Model of the Balloon . . . . .	31



## FOREWORD

This paper describes a three part program which assessed the pre-flight performance of a passive satellite communications system, the thin-wall-stressed-skin passive satellite (Echo II) and the correlation of post-flight data with pre-flight predictions.

A most useful technique has been evolved for evaluating the backscatter characteristics of a small segment of large (135-foot diameter) spherical or lenticular structures in terms of inherent physical distortions based on their physical constructions and the resultant scintillation and communications distortions. These immediate and critical evaluations yield data sufficiently detailed and accurate to construct theoretical models to account for observed scintillations and periodicities from applications of theories of physical and geometrical optics.

The second program phase, prior to flight, evaluated full size inflated Echo II spheres to demonstrate the relationships between the skin-stress-scintillation-level backscatter qualities for actual balloons, since distortions were expected due to telemetry beacons and reinforced panels. Direct r-f backscatter measurements for monostatic and (30°) bistatic angles at two frequencies (2 Gc and 6 Gc) were compared with computed scintillation levels based on stereo photographs and topographical contour maps representing the balloon surface. These data were in good agreement with the techniques of measurement of spherical segments extracted from full size balloons. Scintillation predictions based on observed backscatter data and computed disposition of phase centers were:  $2.0 \pm 1.0$  db (peak values) at 2 kMc and  $5.9 \pm 0.3$  db (peak values) at 6 kMc. These data were valid for monostatic and bistatic angles (30° max), as computed in anticipation of the look angles expected for ground terminals spaced across the United States.

As a consequence of the resultant limits of measured and computed scintillation levels and maximum scintillation rates of less than 10 cps based upon the trajectory least time and observation periods, the Echo II balloon was deemed worthy of launch, and consequently, was launched on January 25, 1964.

This third program phase, including twenty operational and experimental radar systems (a cooperative program including U. S. Dept. of Defense installations throughout the world as well as British Ministry of Aviation (RRE Malvern) and Canadian DRTE, etc.), provided frequency coverage from VHF (400 Mc) to X Band (10.0 kMc) and real time records as well as digitized tape radar records as monitors of the backscatter qualities of the Echo balloon from a few hours after injection into orbit until December 1964. Particular emphasis was required for daily and pass-by-pass observances prior to, during, and post-eclipse passes to determine changes in balloon quality as a consequence of severe temperature change for the satellite. All radar data were recorded in analog form for quick reference and digital tape records for which computer run data-reduction programs were consequently written. These programs revealed systematic scintillations with reference periodicities (since the Echo II sphere was found to be spinning about an inertially stable axis with a period of 100 seconds based on first radar data), higher order periodicities, power spectrum analyses, and mean, average and statistical reduction of scintillation levels. A statistical prediction of bit error rates and signal "dropout" levels below useful levels as limiting bandwidth requirements for communications was the basis for computations which predict the useful frequency bands for communications in terms of the particular modulation techniques employed.

Radar data further enabled the balloon surface to be "mapped" according to calculable symmetrical distortions (such as produced by the two masses of telemetry beacons affixed to the balloon skin), large asymmetrically distorted areas related to large columnar wrinkles, regular wrinkling of the balloon surface, changes of radii of curvature, and comparative qualities of various portions of the balloon. These extraordinary effects, as revealed by radar data (such as delayed radar returns, visible beyond the return pulse limit), were examined on the basis of "holes" which might have permitted excitation of a resonant cavity (or "echo box"), the examination and rejection of the presence of a plasma around the balloon, and the possibility

of multipath radar returns. Such effects, as cited, were examined by fitting geometric perturbations, which under electromagnetic excitation could provide acceptable or non-acceptable explanations to fit the radar records.

It is possible to determine the spin axis orientation of the balloon from radar observations and, in conjunction with beacon records, to compute the spin axis location in inertial space.

In addition to the examination of the Echo II system, the radar establishments were asked to observe both Echo II and the earlier Echo I in sequence for comparative qualities, as Echo I has been in orbit since 1960. Echo I represents a non-stressed spherical system and Echo II represents a stressed-skin-rigidized membrane at discrete pressure. Comparative data indicate that Echo I and Echo II peak scintillation amplitudes were comparable; however, for the former, the scintillation frequencies were higher and signal depressions were of greater duration. The Echo II effective backscatter area is measured at  $31 \text{ db} \pm 1 \text{ db}$  against the calculated value of  $31.2 \text{ db/m}^2$ ; the Echo I system is degraded 8 db below its expected return area of  $28.6 \text{ db/m}^2$  (at injection into orbit).

What has been evolved during this part of the program is significant to the design of succeeding systems. The design of passive satellite communications systems cannot be predicted by extrapolating to large spherical systems by measurement of smaller diameter spheres of the same materials; i.e., because the membrane thickness to date has not been scaled. Also, the time-variant structural deformations of the thin membrane are dependent upon thermal stresses in the structure and distortions due to spin (since both Echo I and Echo II spheres are spinning at a 50 sec period and 100 sec period respectively). The electromagnetic responses are, therefore, critically dependent on the final surface quality presented to the evaluating radar/communications systems.

A basic measurements program has been evolved, which can by measurement of judiciously defined spherical segments, economically and easily measure the parameters of response on segments of reasonable dimensions, and from which, valid extrapolations of electromagnetic responses can be made; therefore, large balloons need not be inflated prior to flight to determine quality as communication devices.

Computer programs have been obtained with which gross data have been reduced, analyzed and assessed for the current program and are applicable to similar future programs. Radar cross section statistics, based on normal and skewed distribution, fading rates probabilities, and monostatic and bistatic behavior effects have been catalogued as aids to data reduction and analysis.

Lightweight open-grid materials, basically to reduce solar pressure perturbations on spherical and lenticular shaped passive reflectors, are now being designed and evaluated economically.

A catalogue of characteristic responses related to distortions, perturbations and shapes has been generated and analytically examined as a means of identification of radar responses so that pre-flight predictions as well as immediate analysis of flight data can be identified.

The anticipated performance of a perturbed, passive-backscatter-spherical system has been computed in terms of fading rates (in carrier power) as functions of frequency thus revealing that the Echo II passive satellite is acceptable at 2000 Mc and higher frequencies employing frequency modulated transmissions, and limited by scintillation-induced noise for amplitude modulations with transmission fading rates of 3 percent at 2 kMc ( $15 \text{ db S/N}$  at receiver) and 0.05 percent at 5 kMc.

# EXPERIMENTAL AND THEORETICAL EVALUATION OF A PASSIVE COMMUNICATIONS SATELLITE (ECHO II)\*

by

A. Kampinsky\*

*Goddard Space Flight Center*

and

R. K. Ritt

*Conduction Corporation*

## INTRODUCTION

This paper describes methods which were developed to predict the radar reflectivity of the Echo II passive communications satellite, and were subsequently used to analyze the data obtained during the first six months of orbital flight.

To illustrate the problem, it should be explained that the Echo II balloon is not a homogeneous, constant-radius sphere but a structure characterized by distinctive areas differing in radius of curvature, flexural strength, conductivity, and finally but not least of all, a random surface roughness.

Figure 1 shows the balloon's structure, wherein 106 panels of a laminate material are brought together at two poles and capped by another layer of laminate material. Two adjacent panels of double thickness run longitudinally through the poles; these are reinforced to accommodate two radio frequency telemetry beacon plaques at the equator. The edges of adjacent panels are joined with a 2.5 cm width of laminate material forming a capacitive coupling. The laminate itself is a

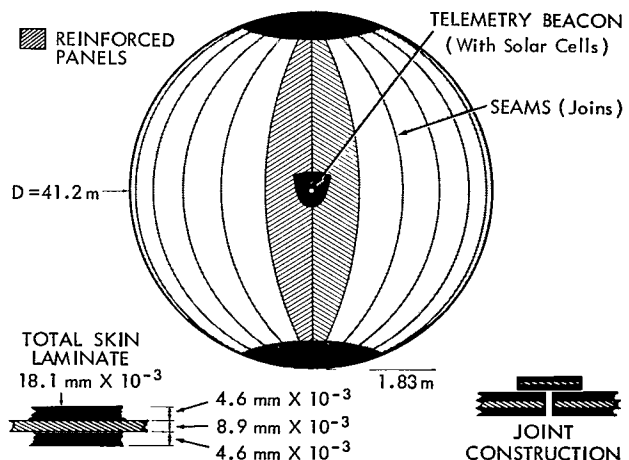


Figure 1—Echo II.

\*Presented at U.R.S.I. 1965 symposium on Electromagnetic Wave Theory, Delft, The Netherlands.

composite of two  $4.6 \times 10^{-3}$  mm layers of aluminum separated by a layer of  $8.9 \times 10^{-3}$  mm polyester film (commercial Mylar).

Thus, the radar cross section of this balloon is not expected to be that of a perfectly conducting sphere 41.2 meters in diameter. The shape of the balloon, which is critical in the determination of its radar cross section, is a function of the internal pressure to which the balloon is subjected during initial inflation and of the degree of rigidization caused by yielding of the aluminum films. The experimental determination of this shape by construction and inflation of a scale model is precluded.

In Appendix A, the differential equations of equilibrium thin membrane theory are shown. These equations lead to similitude conditions which cannot be practically achieved. The alternatives for developing predictions of the reflectivity of the full-scale balloon are the following:

- (1) Inflate a full-scale balloon and measure its radar cross section.
- (2) Inflate a full-scale balloon, measure its surface contours, and compute the radar cross section.
- (3) Using measured values of the properties of the balloon material, construct a theoretical model of the balloon shape, and from this, compute the radar cross section.
- (4) Mount small circular segments, cut from the full-scale balloon in such a fashion that their contours, under uniform pressure, will be the same as they would be in flight. Then perform radar cross section measurements and/or compute the radar cross section from contour measurements of these mounted segments.

All of these alternatives were tried during the program. Each one has special problems, depending on the validity of special assumptions. Nevertheless, the results of these separate methods of prediction were consistent, thus providing verification of each other. A catalogue of characteristic radar responses related to balloon distortions and perturbations was analytically examined so that preflight predictions as well as immediate analysis of flight data could be compared. Further, the communications performance of such passive, backscatter type satellites was analyzed.

In the following text, the prediction program is summarized, and the use of the resulting knowledge to evaluate the flight test balloon is described.

## **SMALL SEGMENT MEASUREMENTS (PHASE I)**

The physical arrangement for measuring small segments is illustrated in Figure 2. The segment, 12 feet in diameter, was rigidly attached to circular ring F and a sealed chamber which could be pressurized behind the segment. The segment could be maintained at a constant pressure level for a period of time while RF measurements were performed, and then relaxed to ambient pressures for comparative measurements.

Mechanical analysis was then performed; the basic assumption was that under very small pressures the seams, being relatively non-elastic, would assume their basic shape of circular arcs having a radius of 20.6 m. Using thin membrane theory, for which the equilibrium equations are given in Appendix A, it was determined that except for an annular *boundary layer* extending from rigid ring F, the segment contour would be identical to its contour in the full-scale balloon at the same value of the tangential stress. The width,  $d$ , of this boundary layer is given by the formula

$$d = r_0 \sqrt{\epsilon} ,$$

where  $r_0$  is the segment radius and  $\epsilon$ , the tangential strain, is computable from the tangential stress, or equivalently (knowing the thickness of the layer), from the internal pressure. In the current case, at the maximum tangential stress of 12,000 psi, the value of  $d$  was 2 ft., leaving an 8 ft. diameter section which would be a replica of the same section on the full-scale balloon.

To justify the procedure electromagnetically, it was determined that at the lower frequency limit to be used in the experiment, 1.7 kMc ( $\lambda = 0.18$  m), the first Fresnel zone for a sphere is determined to be a circular segment having a chordal diameter of 2.7 m. It was then reasoned that the radar cross section contribution from the remainder of the balloon would be negligible compared to the nominal cross section  $\pi R^2$ , unless the balloon were so badly distorted from its spherical shape that specular scattering centers would exist exterior to the first Fresnel zone. Consequently, relative to the nominal cross section, the radar cross section (RCS) of the small segment would be the dominant contribution to the RCS of the full-scale balloon, and the scintillation effects would be preserved.

This conclusion was conditional, on the assumption that the RCS contribution of the abrupt electrical termination of the 12 ft. diameter segment could be minimized. To accomplish this, a flange (FGE on Figure 2) was constructed to match the tangential plane to the segment at the termination F, and to direct electromagnetic energy arriving in this region away from the back-scattered direction. The flange was designed so that the creeping wave launched at G would be sufficiently dispersed and the energy returned from the flange termination (assuming total reflection) would have an RCS contribution of at least 20 db below that of the nominal balloon cross section.

Measurements were obtained by operation of a cw radar assembly at 1.7 kMc and 5.8 kMc for monostatic views as well as bistatic-look angles as a transmitter cart was moved across a 30°

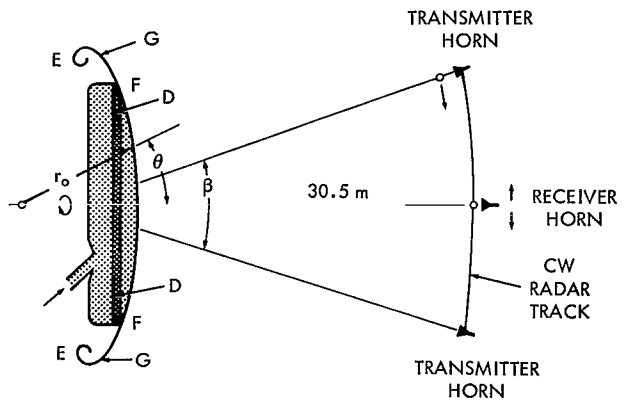


Figure 2—Spherical segment.

track at 30.5 meters from the support of the spherical segment. The measurements were recorded and were essentially the scintillations obtained as functions of angular aspect with the variables introduced as follows:

- (a) Two frequencies
- (b) Two orthogonal polarizations
- (c) A pressure range from ambient level to 12,000 psi and cycled back to ambient (to reveal the minimum stress level indicative of a permanent strain condition).

The RCS was corrected to obtain the "far field" cross section values since measurements were performed, of necessity, in the "near zone". This correction was determined to be  $(1 + a/2r)^{-2}$  where  $a$  is balloon radius and  $r$  is the distance from balloon segment to the receiver (References 1 and 2). From the characteristic scintillating responses, more than one specular point is to be observed. Inasmuch as the balloon behaved as a series of spheroidal members with radius of curvature  $a_1$  in the meridian planes differing from radius  $a_2$  in the latitude planes, the spherical segments as measured, and subsequently the total balloon in flight, exhibited characteristic scintillation rates which were quite predictable. To substantiate the membrane analyses, contour measurements were also obtained by measurement from a reference plane tangential to the spherical segment to the material, under various pressure levels. Although it would have been preferable to have evaluated the Kirchoff integral by numerical techniques, it was felt that the precision of contour measurements was not sufficient to make this procedure meaningful. Therefore, the RCS was approximated by using the specular formula  $\pi a_1 a_2$ . (At later time in the program during radar backscatter measurements of the full balloon, numerical integrations were employed in conjunction with better contour measurements evolved from stereo photographs). Figures 3a-3c illustrate the data obtained.

As a result of the small segment measurements, it was concluded that:

- (1) The mechanical behavior of a circular segment cut from a full scale balloon can be simulated by mounting the segment on a circular structure. Care must be exercised in determining the boundary conditions for which the simulation is biased.
- (2) By correctly providing for electrical termination, the radar cross section of the full scale balloon can be measured by performing measurements on the circular segment.
- (2a) The average cross sections measured, when extrapolated to the far zone, will be accurate to within  $\pm 1$  db, and will be highly correlated with the specular values obtained from contour measurements.
- (2b) The scintillation measurements as a function of aspect are too restrictive unless a segment of approximately 20 feet in diameter is used. Concurrently, the theoretical determination of these scintillations must be performed by numerical evaluation of the physical optics integral in conjunction with accurate contour measurements. Figure 3a gives the range of cross section data, at 1.7 kMc, for pressures ranging from 700-12,000 psi, compared to the range predicted by the contour measurements. Figure 3b

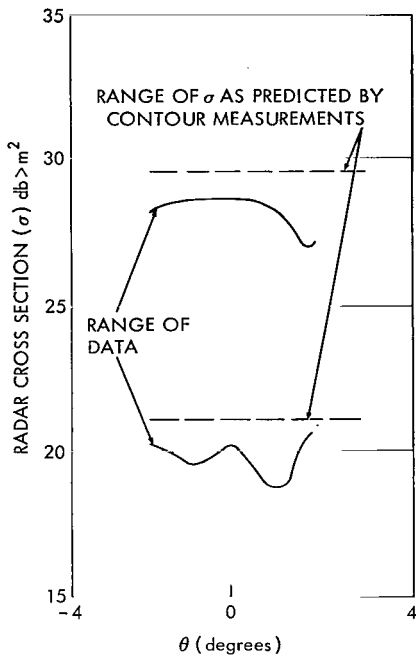


Figure 3a—Range of cross section data at 1.7 kMc.

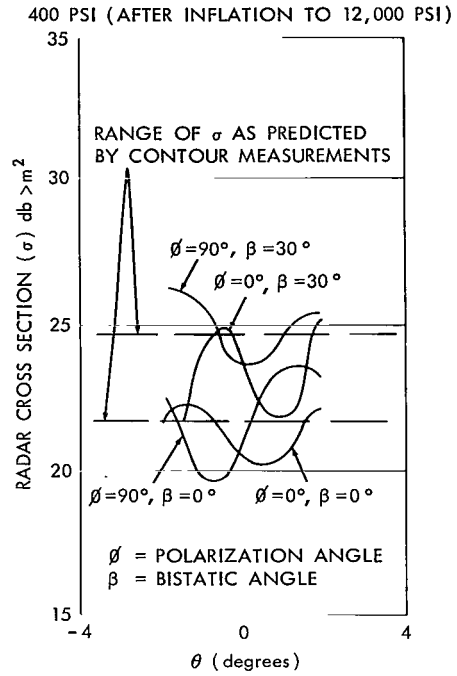


Figure 3b—Comparison of the range for the final relaxed condition.

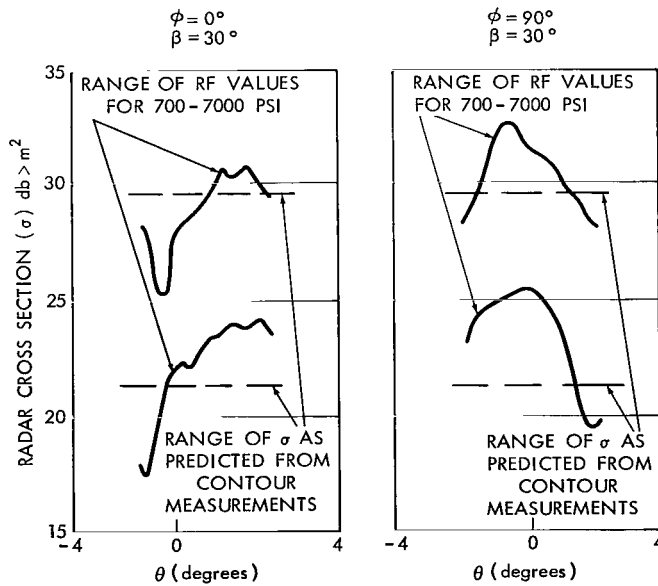


Figure 3c—Comparison of the ranges at C-band frequencies for a bistatic angle of 30°.

compares the ranges, for the final "relaxed condition", for both polarizations and bistatic angles of  $0^\circ$  and  $30^\circ$ . Figure 3c is a similar comparison for a bistatic angle of  $30^\circ$  for two polarizations at C-Band frequencies.

- (3) For the Echo II material supplied for this program, the average far zone cross section varies between  $30 \text{ db} > \text{m}^2$  and  $34 \text{ db} > \text{m}^2$  as the pressure is increased from 700 psi to 12,000 psi. The average cross section decreases as the pressure increases. Upon relaxation, the cross section patterns more closely resembled the high-pressure measurements, rather than the low-pressure measurements, indicating a rigidization of the material at some intermediate pressure. No significant dependence of the average cross section on either frequency, polarization, or change in bistatic angle was observed. However, a noticeable variation in cross section from gore to gore was noticed, indicating deviations of the gore surface from a nominal radius. In actuality, this lack of uniformity was of the order of several inches, but the resulting variation in local radii of curvature created a much greater variation in radar cross section than had been anticipated prior to the initiation of the program.

It should be noted that, currently, investigations of possible passive satellite materials are being conducted using a 22 ft. segment, with an inflatable torus replacing the rigid mounting ring. This arrangement permits more precise control of the radius of curvature.

## **MATHEMATICAL MODEL OF THE BALLOON**

A highly simplified model of the balloon was postulated, and is described in Appendix B. Basically, the individual zones were represented as having a constant radius of curvature in the longitudinal direction, and for each value of latitude, a constant radius of curvature in the latitudinal direction. The ratios of these two radii vary from about 1 (corresponding to a surface stress of 12,000 psi) to 22 (corresponding to a surface stress of 500 psi). These values were computed from mechanical data that had been obtained in previous laboratory studies of the Echo II material. It should be observed that going from a ratio of 1 (perfect sphere) to a ratio of  $\infty$  ("flat" panels) involves a change in the radial distance of only 1% of the nominal 20.6 meters.

The resulting radar cross section pattern, as a function of azimuth, is highly sensitive to frequency, pressure, and latitude. The fields were computed numerically, using the formulation as an incomplete Fresnel integral, and described in Appendix B. Typical predictions are shown in Figure 4a and 4b.

## **FULL SCALE BALLOON (PHASE II)**

To further explore the analytical techniques, three actual Echo II balloons were inflated in a dirigible hangar at the Naval Air Station, Lakehurst, N. J., between July and December 1962.

The principal data to be obtained were:

- (a) Stereo photographs of portions of the balloon from which topographical feature plots of the surface could be derived (all of these to be correlated with carefully controlled pressure levels).
- (b) Radio frequency measurements. A continuous wave radar system was set up so as to illuminate the balloons at a position diametrically opposite that of the stereo photographic site. The disposition of equipment was equivalent to that employed to illuminate the spherical segments. A segment of circular track, arranged at a radius of 30.5 meters from the balloon, permitted an automatically driven receiving horn system to move at constant rate so as to receive in either a monostatic or bistatic mode. Figure 5 shows the physical disposition of equipment.

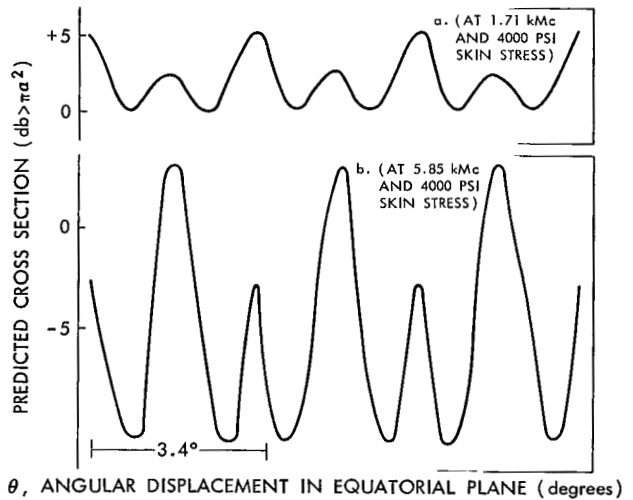


Figure 4—Predicted cross section of balloon ( $db > \pi a^2$ ) versus angle  $\theta$  (at 1.71 and 5.85 kMc and 4000 psi skin stress).

Again, polarization selection was employed at both frequencies of 1.7 kMc and 5.85 kMc during the variation of pressure levels from ambient level to burst level.

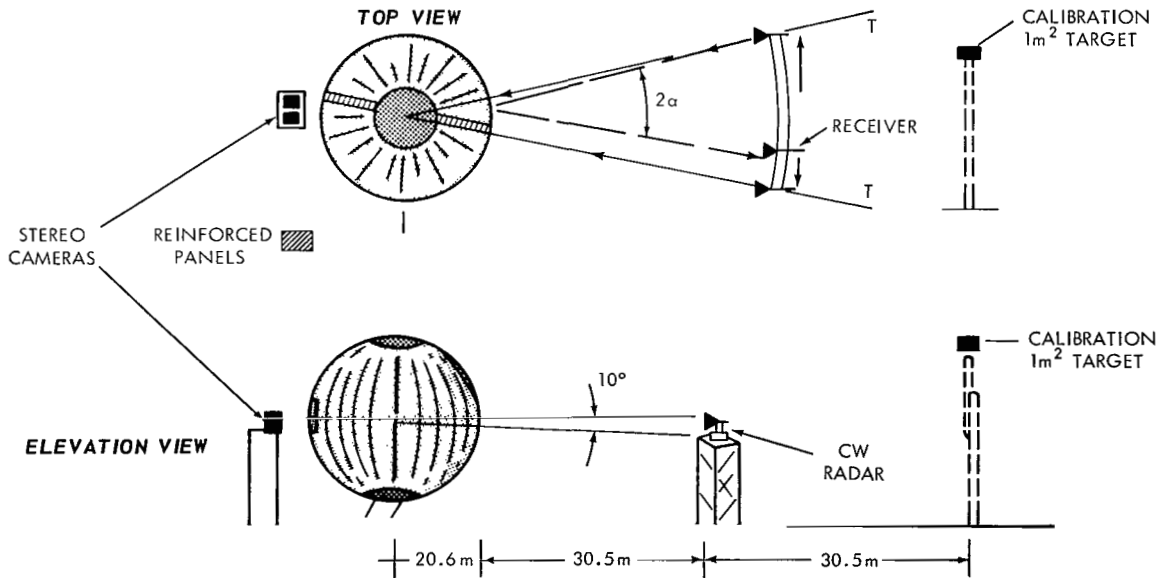


Figure 5—Stereo camera and radar setup, balloon in hangar.

Prior to setting up of the balloon in the hangar, backscatter surveys were recorded for the bare interior. This was accomplished through placement of high gain narrow beam antennas at the proposed balloon center and backscatter from walls, columns, and ceilings and were recorded at selected receiving positions. The data showed that, if the balloon were under-illuminated by approximately 10 db at the tangential regions, and if the shielding of the balloon itself were taken advantage of, a dynamic recording range of between 25 and 30 db could be expected for both frequencies. Further, as shown in Figure 5, a calibration plate of one meter square area surrounded by absorbing material was arranged as an absolute reference.

The physical arrangement permitted stereophoto data, viewing a region  $10' \times 17'$ , to be recorded throughout the pressure levels from ambient level to maximum while radar measurements were performed.

Inasmuch as a catalogue of characteristic backscatter data was collected to identify the surface characteristics of the Echo balloon in flight, the first correction necessary was that needed to correct for the location of the balloon for *near zone* operation using both monostatic and bistatic angles of view.

As in the case of the segment measurements, the data were corrected to account for the fact that the measurements were taken in the near zone of the balloon. For the particular measurement parameter being used, this correction required the data to be increased by 4.5 db. An additional correction, needed for the bistatic measurements, was made to account for the beam taper of the receiving and transmitting horns.

Figures 6a-6d are typical of the raw data obtained. Each pattern represents the RCS over a  $15^\circ$  region of the balloon (Figure 5). The data in Figure 6a were taken at 5.85 kMc, with the initial skin stress level of 400 psi.

Figure 6b shows data taken at 5.65 kMc, with a skin stress level of 7500 psi. Figure 6c presents data taken at 5.85 kMc, with the balloon pressure relaxed to ambient after inflation to 7400 psi skin stress. Figure 6d contains data taken at 1.71 kMc, with the initial skin stress of 400 psi.

Figures 6a, 6b, and 6c illustrate changes in the nature of the scintillations both as the pressure is increased and then relaxed after rigidization has taken place. Figures 6a and 6d should be compared to see the frequency dependence of the scintillation behavior.

These recordings show that rigidization occurred at a skin stress level between 3200 and 7200 psi. On this basis, it was recommended that a balloon be stressed to at least 4800 psi in orbit.

The data was reduced to determine systematic dependence upon the varying parameters. Of particular interest is the observation that the RCS has negligible dependence upon polarization. The distribution functions were computed for the difference,  $\Delta$ , between maximum and minimum values of the RCS on  $5^\circ$  intervals. At  $\sim 6$  kMc, the maximum of this distribution occurs at 5 db,

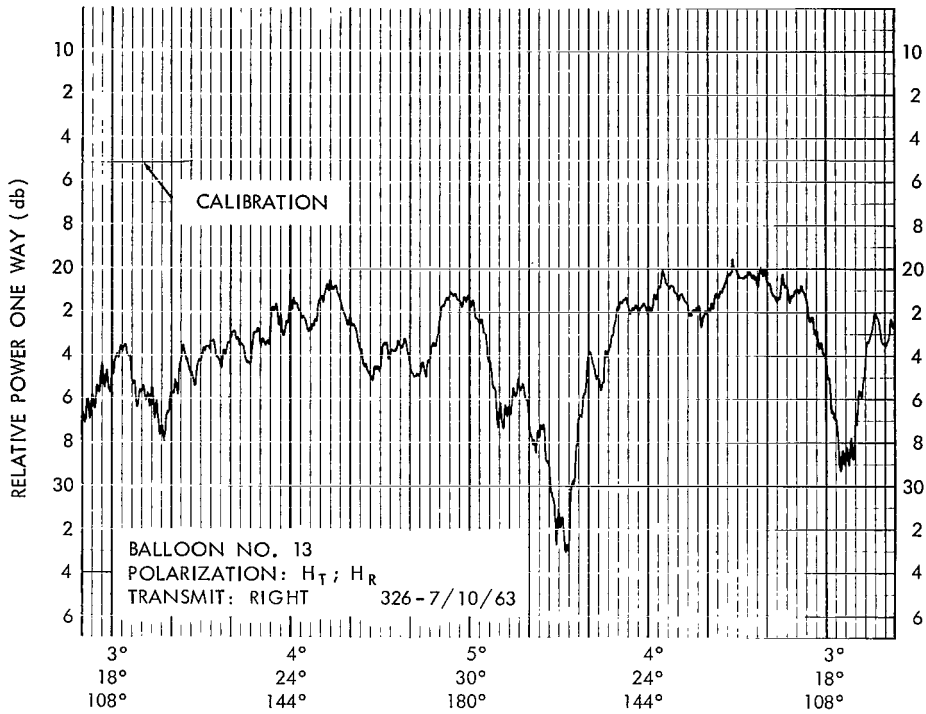


Figure 6a—The radar cross section at 5.85 kMc and 400 psi.

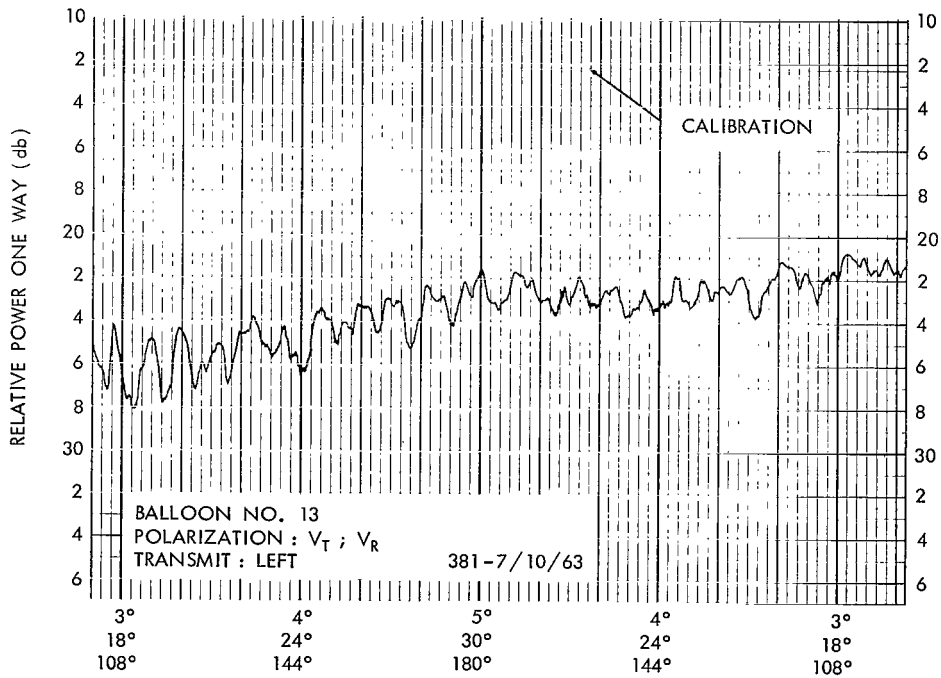


Figure 6b—The radar cross section at 5.65 kMc and 7500 psi.

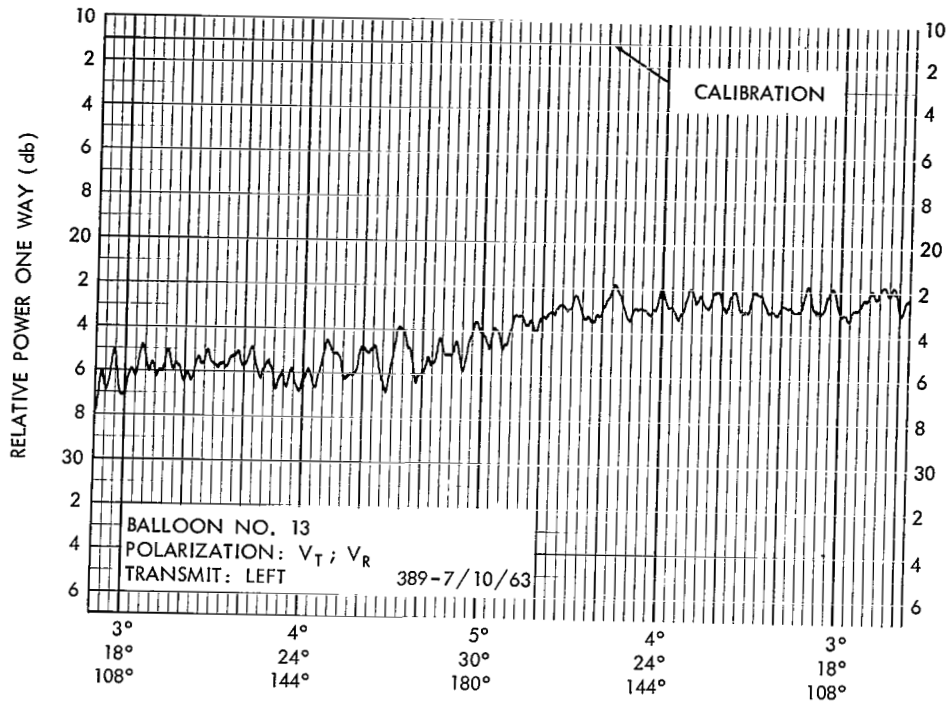


Figure 6c—The radar cross section at 5.85 kMc and relaxed after 7400 psi (non-reinforced panels).

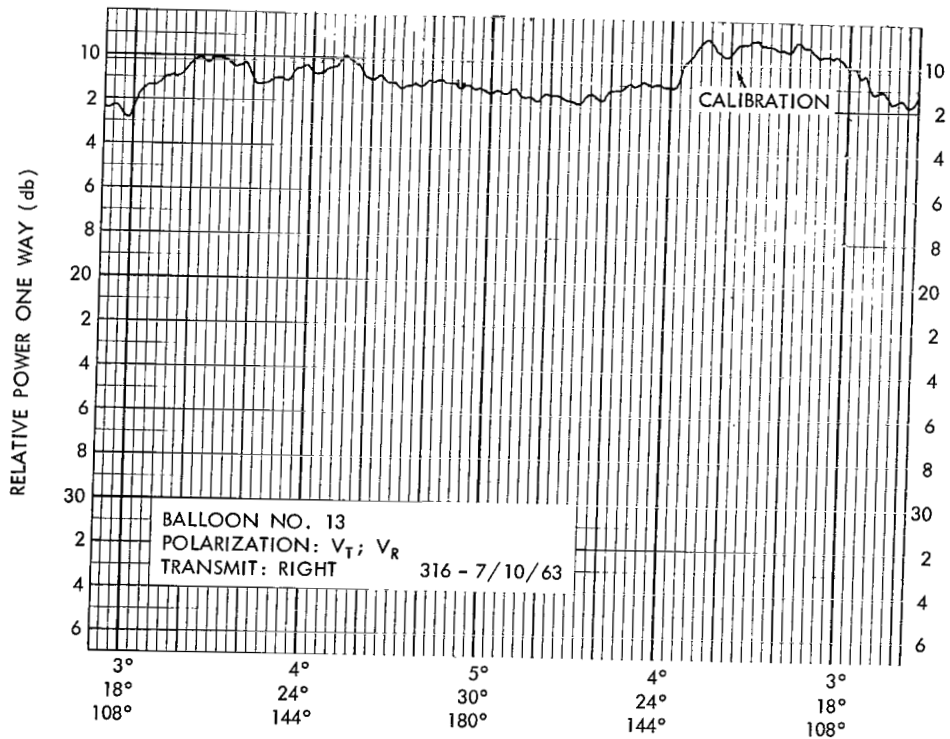


Figure 6d—The radar cross section at 1.71 kMc and 400 psi (reinforced).

with most of the values between 5 and 6 db. At approximately 2 kMc, the maximum occurs at 3 db, with most of the values between 2 and 4 db. To determine periodicities, autocorrelation functions were computed for angular increments of 0.5 degrees.

Figure 7 shows typical autocorrelation curves which were computed for bistatic look-angle  $\beta$  and the RCS distribution from data shown in Figures 6a, 6b, 6c, and 6d. These curves reveal that the autocorrelation function depends mainly upon radar frequency, and is not very sensitive to pressure, polarization, or location on the balloon.

This indicates that the basic "panel" structure determines the spectrum of the RCS as a function of aspect. At the higher frequency there is a well-defined-autocorrelation peak at  $5^\circ$  and at  $10^\circ$ , which, because of the bistatic measurement, corresponds to  $2.5^\circ$  and  $5^\circ$  on the balloon. Close scrutiny of Figure 4, at 5.85 kMc, discloses periodicities of these orders of magnitude.

The photogrammetric data were reduced to supply contour maps of the form shown in Figure 8. From these maps, using physical optics and numerical integration, the radar cross section was computed (Figures 9a and 9b). Comparison between these calculations and the measured data reveals that the scintillation levels are highly correlated at all frequencies and pressures, whereas the mean cross section is closely correlated at the higher pressures.

### PRELUDE TO THE ORBITAL BALLOON (PHASE III)

The theoretical analyses and the experimental work described in the preceding sections lead to the conclusion that a guide line has been provided to the values of RCS and the nature of scintillations to be expected. In particular, if the skin stress level were to exceed 7000 psi, a mean RCS of about  $30 \text{ db} > \text{m}^2$  would be achieved, with a scintillation level between 4 and 8 db for frequencies up to 6 kMc. If this value of skin stress were not to be achieved in the orbital balloon, the radar cross section return would serve to determine what state of surface quality had actually been achieved. As a consequence of the accumulated information, the Echo II balloon was deemed worthy of launch, and consequently, was launched on 25 January 1964.

It was decided that during the orbital flight radar data would be collected, reduced, and analyzed. The acceptance of data was predicated upon its reproductivity with respect to a large number of radar sites and observers. It was also predicated that explanation of "anomalous" behavior of the radar, i.e., gross departure from the accumulated, or reference data, would be attempted only by application of the known laws of nature.

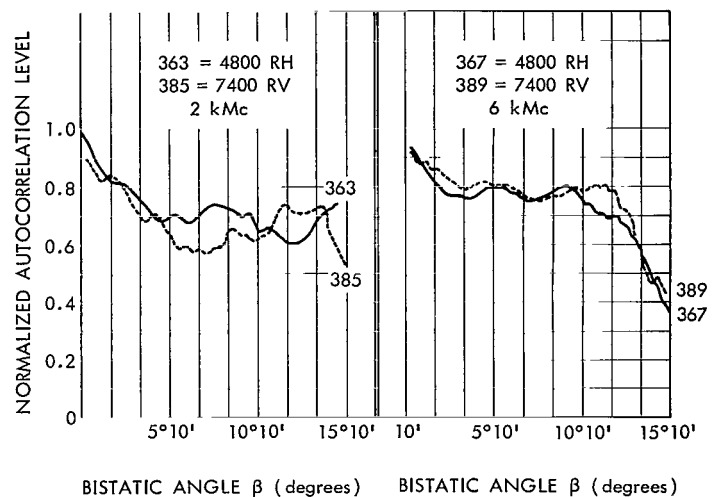


Figure 7—Autocorrelation curves.



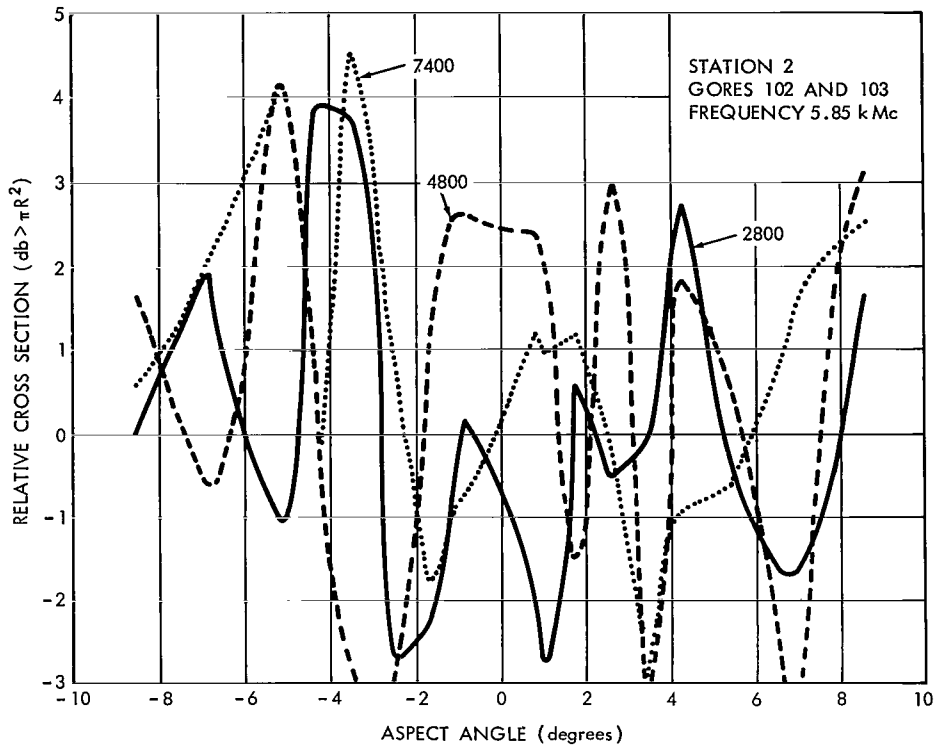


Figure 9a—Computed cross section from photogrammetric measurements over a  $16^\circ$  aspect interval.

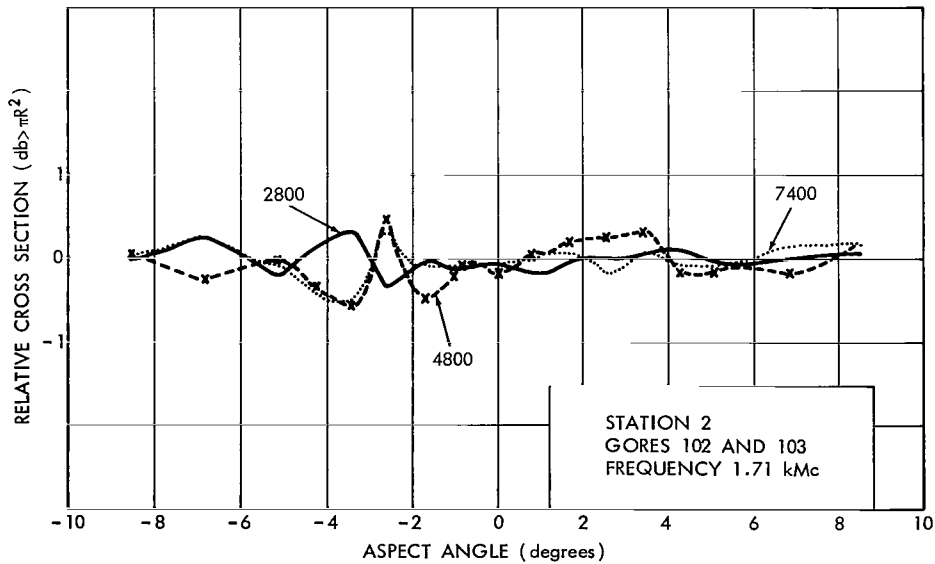


Figure 9b—Computed cross section from photogrammetric measurements over a  $16^\circ$  aspect interval.

Table 1  
Radar Facilities

Station	Cognizant Agency	Location	Frequency (band)	Peak Power (Mw)	Pulse Length ( $\mu$ sec.)	PRF	Beam Width	Antenna Size (feet)	Antenna Gain (db)	Polarization
Antigua	AMR	Antigua	C	2.8	.25-2.4	160	0.43°	29	51	Vert-Hor-Cir
Aris Ship (Gen Arnold)	AMR	Ascension Isle	C	1	30	160	0.4°	30	52	Hor-Vert
			L	10	30	160	1.5°	40	41	Hor-Vert
			X	1	30	160	0.4°	40	52	Hor-Vert
			C	1	30	160	0.4°	30	52	Hor-Vert
Aris Ship (Gen Vandenburg)	AMR	Cape Kennedy	L	10	30	160	1.5°	40	51	Hor-Vert
			X	1	30	160	0.4°	40	52	Hor-Vert
			S	25	7	125	0.24°	60	51.5	Hor
Cornell Radar Labs	Cornell U	Buffalo, NY	S	25	7	125	0.24°	60	51.5	Hor
Grand Turk	AMR	Grand Turk Isle	C	2.8	.25-2.4	160	0.43°	29	51	Vert-Hor-Cir
Malvern	RRE	Malvern, England	S	3	10	200,180	0.5°	45	50	Lin
Milstone	L. L.	Westford, Mass.	L	5	2	15	1.3°	84	46.5	Cir
Patrick AFB	AMR	Patrick AFB, Fla.	C	2.8	.25-2.4	160	0.43°	29	51	Vert-Hor-Cir
Wallops UHF	L. L.	Wallops Isle	.42-4.5 kMc	8	2	30	2.6°	60	36	Vert-Hor
Wallops S	L. L.	Wallops Isle	S	5	2.2	320	0.39°	60	52.8	Vert
Wallops S	NASA	Wallops Isle	S	5	1, 2, 5	256, 303 328, 390	0.39°	60	52.8	Vert-Hor-Cir
Wallops C	NASA	Wallops Isle	C	2.8	.25-2.4	160	0.43°	29	51	Vert-Hor-Cir
Wallops X	L. L.	Wallops Isle	X	1	2.5	320	0.12°	30	60	Vert

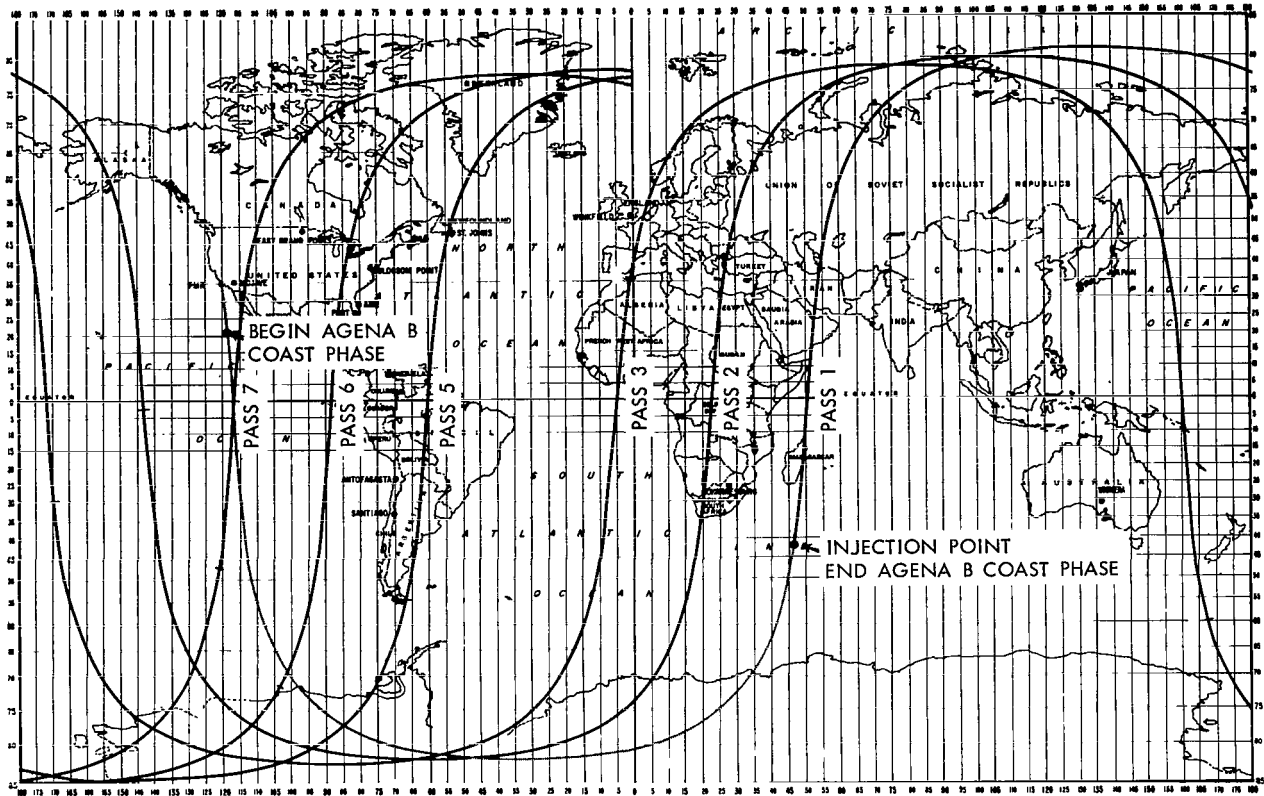


Figure 10—Sub-orbital plot of Echo II satellite.

Of particular interest to radar observers was the intent to observe the Echo balloon prior to entering the earth's shadow (after eleven days of full sunlight), during this eclipse, and post eclipse, and the effects of heating and cooling on the balloon radar quality. Radar observations were to be intensive during the first weeks of flight (the initial pressurization occurring thirty minutes after the balloon was ejected from its canister) and until nearly one year later in December 1964.

## ECHO II ORBITAL FLIGHT RADAR DATA AND ANALYSIS

Scintillation of the radar returns was observed immediately after the first pass. Subsequent radar data could be related to internal pressure levels and tangential skin stress values equivalent to no more than 1000 psi. The expected value was 5000-6000 psi. A second major unexpected result was evident in a repetitive RCS drop with a 100 sec period, which indicated that the Echo II balloon was rotating about an inertial axis with a spin period of 100 seconds.

As more data were collected, further anomalous behavior was exhibited, some detectable in the analog records and some, not detectable by the eye, were revealed by the magnetic tape

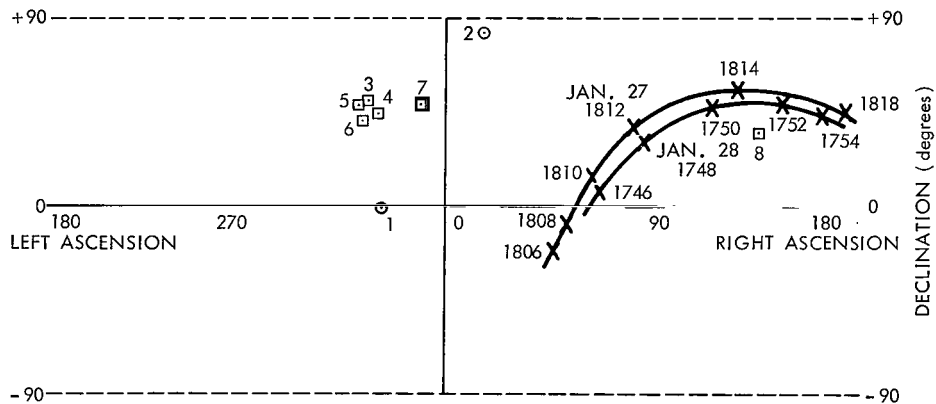
recordings. The total inferential behavior of the Echo II balloon was also compared with the Echo I, the 100 foot diameter sphere launched in 1960.

As the radar data accumulated, they were examined visually when in the form of analog recordings and processed digitally when in the form of computer tapes. The following behavior was consistently observed:

- (1) The scintillation amplitudes, the autocorrelation functions, and the mean cross sections continued to be typical for a balloon inflated to a tangential skin stress of 1000 psi.
- (2) The spin period continued to be  $100 \pm 5$  seconds. The periodically depressed RCS values, upon which this estimate of the spin rate was based, continued to be observed.

An analytic program to determine the spin axis orientation in vertical space was instituted. The basic data used for this determination was the telemetry-beacon-pattern data supplied by the RRE, at Malvern, England. In conjunction with this calculation, various observers noted a "flattening" or "smoothing" of the RCS scintillations for particular radar look-angles. By hypothesizing that this smoothing was coincident with looking along the spin axis, an estimate of the spin axis coordinates was made. Figure 11 shows comparisons among these variously obtained spin axis coordinates.

An additional bonus was derived from the Malvern data. The periodic drop in the RCS data occurred at the position of the telemetry beacon mass, which in turn, was located on the reinforced panels of the balloon. This location provided an important clue to the



SPIN AXIS DETERMINATIONS

POINT	STATION	DATE	METHOD	POINT	STATION	DATE	METHOD
1	MALVERN	JAN. 27-28	CALCULATION	5	PRINCE ALBERT	JAN. 28	RADAR
2	MALVERN	JAN. 27-28	CALCULATION	6	PRINCE ALBERT	JAN. 30	RADAR
3	MALVERN	JAN. 25	RADAR	7	PRINCE ALBERT	JAN. 30	RADAR
4	PRINCE ALBERT	JAN. 27	RADAR	8	AIR FORCE	MAR. 25	RADAR

Figure 11—Spin axis determinations and Malvern flight paths.

probable cause of the major RCS drop, namely, a wedge-like deformation of the balloon. Calculations were performed to determine the effect on RCS levels of such a wedge, and the *wedge response* was found to be consistent throughout the radar data.

- (3) The observed radar data had a *spikey* appearance when compared to the segment and full scale balloon measurements. This quality of the data is reminiscent of sea radar data returns and similar to results of transmission through plasma. A simple mechanical analysis shows that vibration modes, incurred by differential displacements of the panel joints caused by balloon rotation, would have frequencies between 1 and 8 cps. This sustained wave-like motion throughout the balloon structure offers a possible explanation for the spikey radar return.

Many observers had advanced theories to characterize the scintillation behavior of the radar data. One suggested that the sublimating material used to inflate the Echo balloon, upon being vented to the balloon exterior, was ionized by solar radiation flux so as to form a plasma of variable density about the balloon. Expected electron densities were of  $10^{10}/\text{cm}^3$  in the immediate vicinity of vent holes to  $10^7$  electron/cm<sup>3</sup> at a distance from the balloon surface equal to the balloon radius. However, any free charges about the balloon must, in interaction with the geomagnetic field at the balloon orbital velocity, diffuse along the magnetic field lines and be swept away by the magnetic field forces, as well as ambipolar diffusion of the ionized gas. A second attribute of the plasma, least likely to produce an invariant well-behaved scintillation pattern week after week, is the amorphous shape of any ionized medium. Further, plasma resonance frequencies for electron concentrations cited would be very near that of the 136 Mc beacon frequencies, hence could be expected to severely attenuate or refract the beacon signals. No such effect was observed.

A most interesting anomaly was observable in the S-band radar data from RRE at Malvern, England. These records showed that, subsequent to the return of the main pulse of 10  $\mu\text{sec}$  duration, a train of exponentially decaying pulses was observed which appeared in time anywhere from 10 to 50  $\mu\text{sec}$  beyond the main pulse. One explanation, offered by RRE, depicts the balloon with a hole 1.5 by 0.5 meters in extent, excited by the incident field, which in turn excited a mode in the balloon; then, by reflection from the inner balloon, re-excited the hole (analogous to the familiar "echo box" effect).

One should consider that, taking into account the 10  $\mu\text{sec}$  pulse width, the balloon must act as a 20  $\mu\text{sec}$  delay line. Since the two-way diameter dimension of the balloon is 52.4 meters, the corresponding delay is 0.27  $\mu\text{sec}$ . This electrical mode velocity is therefore 1/80 of free space velocity, or 270 internal reflections, wherein the principal mode has a velocity  $1/\sqrt{2}$  of free space, as derived from geometric optics. The *echo box* explanation is considered invalid since very high order modes need to be excited and sustained, and no lower order modes are to be excited. No other S-Band radar or data of lower or higher frequencies than S-Band show this repetitive phenomenon.

Somewhat similar gross effects of signals appearing after cessation of main pulse are attributable by their observers to multi-path phenomena associated with low elevation angle

observances. Intensive examination of these records show that these effects were observed both at high and low elevation angles.

The possibility of a recognizable circular or elongated hole and material flap, as might be produced by a collision between the balloon and the two halves of the canister (from which the balloon was originally ejected), was considered in detail. Computations indicated that the canisters in their proper trajectory, would appear to cross the balloon trajectory but would be separated by a distance of 2000 to 5000 meters, however, no collision is believed to have occurred. No radar data substantiates the existence of holes or tears in the balloon of such dimensions as to be recognizable as radar data of identifiable format. Instead, the radar scintillations of the Echo II appear to be primarily related to skin stress of 1000 psi, distortions imposed by balloon rotation, and concentrated surface masses (such as telemetry beacons) surrounded by wrinkles parallel to the gore seams, predominately at the balloon equator and exhibiting cylindrical geometry.

In addition to the examination of the Echo II system, the radar establishments were asked to observe both Echo II and the earlier Echo I in sequence for comparative qualities. Echo I, in orbit since 1960, represents a non-stressed spherical system, and Echo II represents a stressed-skin rigidized membrane at discrete pressure. Comparative data indicated that Echo I and Echo II peak scintillations amplitude were comparable; however, for Echo I the scintillation frequencies were higher and the signal depressions were of greater duration. Echo II effective backscatter area is measured at  $31 \pm 1$  db against the calculated value of  $31.2 \text{ db} > \text{m}^2$ . The Echo I system is degraded 8 db below its expected return area of  $28.6 \text{ db} > \text{m}^2$  (at injection into orbit). Figures 12a and 12b present a comparison of data from Echo I and Echo II.

## EFFECTIVENESS AS A COMMUNICATION SATELLITE

Quantitative questions have been examined in connection with the effect of variations in the Echo II RCS (radar cross sections) regarding functional use of the balloon as a passive communications satellite. The findings depend upon present understanding of the statistical properties of the RCS.

On the basis of computations performed below using Echo II as part of a typical system of fixed antenna dimensions, power levels and range, and with frequency choice as a variable, it is concluded that:

- (a) Fading rates (in carrier power) are unacceptable for high quality communication at UHF, marginally acceptable at 2 kMc and acceptable at 5 kMc. In practical terms this means that the Echo II is suitable for frequency modulated transmission at carrier frequencies greater than 2 kMc.
- (b) Radar cross section scintillation of the Echo II introduces noise into the information channel for amplitude modulated signals. For amplitude modulated voice transmission, this noise can be expected to significantly degrade quality; however, the noise can be expected to be negligible for telegraphic or slow data rate communication.

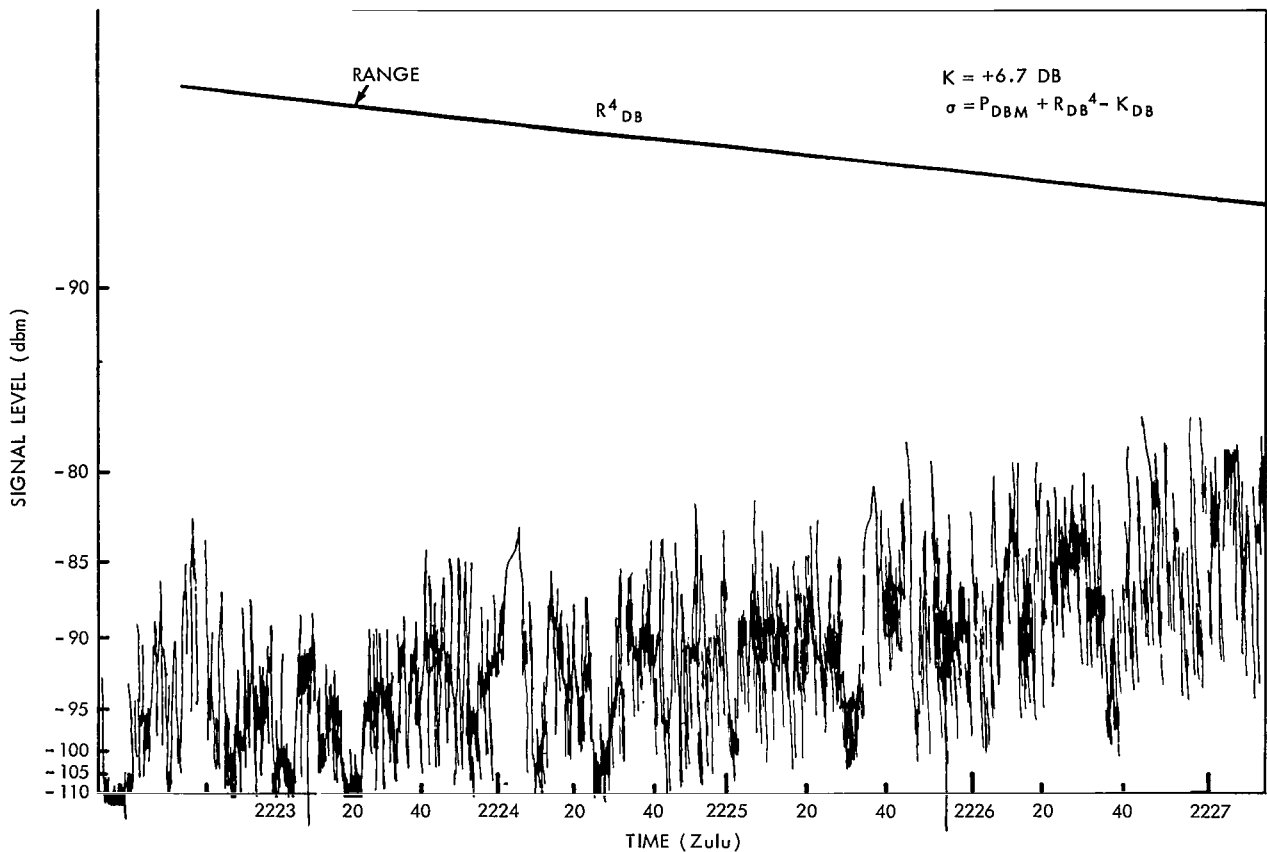


Figure 12a--Radar return from Echo I at S-band, 26 May 1964, FPS-18 radar.

For high quality speech transmission with a 20 Kc bandwidth, the following system parameters have been postulated:

- Noise temperature: 1000° K
- Signal/Noise Figure: 25 db
- Antenna diameter (receiver and transmitting): 60 ft
- Transmitting power: 1 Kw
- Modulation: FM

If  $\sigma_m$  is the minimum balloon cross section required to obtain the 25 db signal/noise figure,

$$\sigma_m \sim 10^3 \lambda^2 ,$$

where  $\lambda$  is the wavelength of the carrier. For a 40-foot antenna, this number would be multiplied by 9/4. This gives the table:

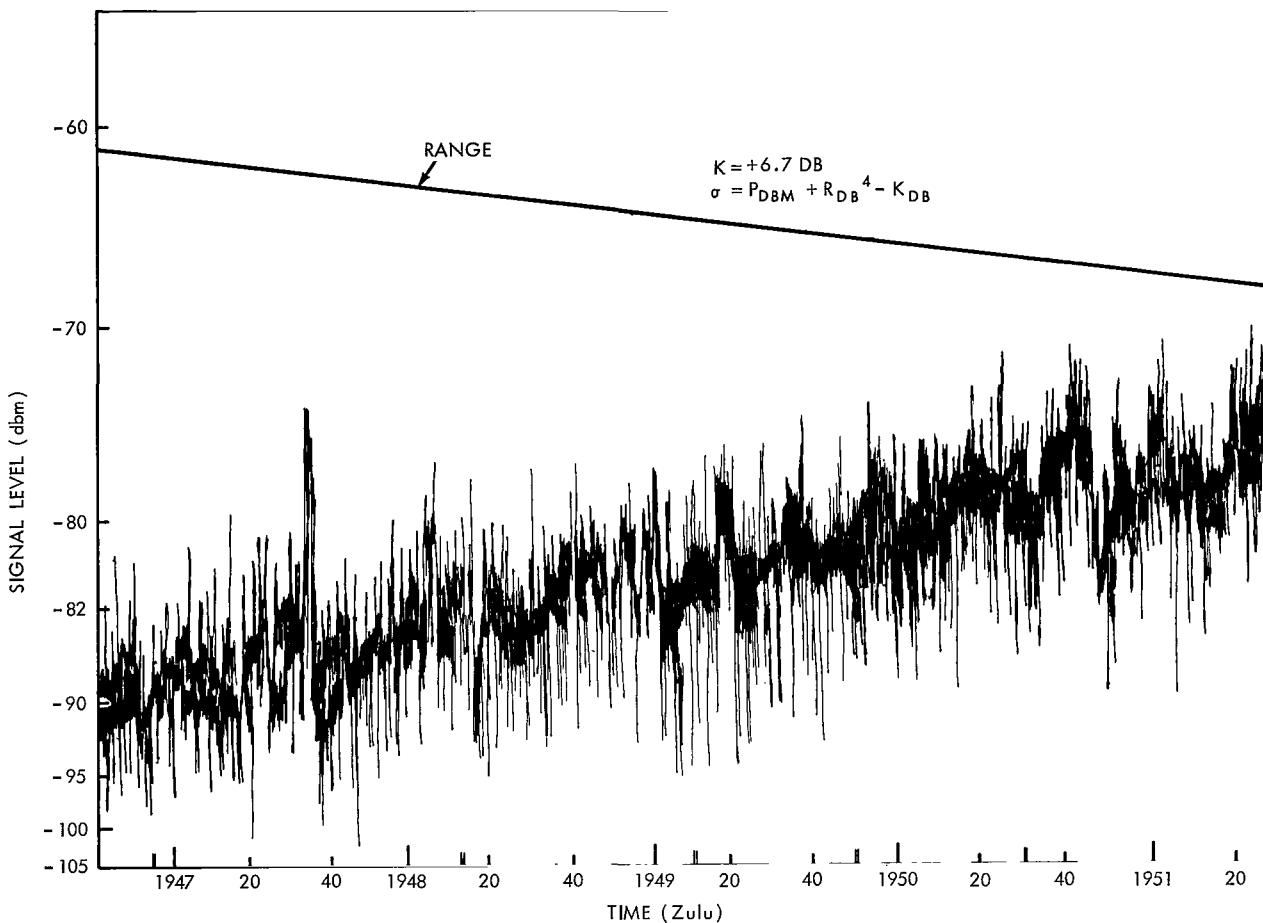


Figure 12b—Radar return from Echo II at S-band, 26 May 1964, FPS-18 radar.

Carrier Frequency	$\frac{\sigma_{min}}{\sigma_0}$ (60-ft antenna)*	$\frac{\sigma_{min}}{\sigma_0}$ (40-ft antenna)*
0.3 kMc	- 1.2 db	+ 2.3 db
2 kMc	-17.7 db	-14.2 db
5 kMc	-25.6 db	-22.1 dg

\*Minimal  $\sigma_{min}/\sigma_0$  to achieve 25 db signal/noise ratio  $\sigma_0 = 1320 \text{ m}^2$  at 1 kw transmission.

From the following table, the fading rate (percentage of time the balloon cross section is less than  $\sigma_{min}$ ) can be computed, assuming that  $A = 6$ , where  $A$  is defined as the one sigma, standard deviation value.

Carrier Frequency	Fading Rate (60 ft antenna)	Fading Rate (40 ft antenna)
0.3 kMc	76%	90%
2 kMc	3%	8%
5 kMc	0.05%	0.5%

It should be noted, however, that the response of Echo II is significantly better, in terms of scintillation peak values, for the lower frequencies than for the higher frequencies.

The value  $A = 6$  used in these computations is conservative. From data observed,  $A$  in general will be smaller, giving lower fading rates.

## Radar Cross Section Statistics

The data obtained for a run of length  $T$  provides a record of the cross section,  $\sigma(t)$ , as a function of time. The mean cross section  $\sigma_0$  is defined as:

$$\sigma_0 = \frac{1}{T} \int_0^T \sigma(t) dt .$$

Let  $f = \sigma(t)/\sigma_0$ . Regarding  $f$  as a random variable, the mean value of  $f$ ,  $\langle f \rangle$ , is clearly unity, and the variance of  $f$ ,  $V_f = \langle f^2 \rangle - 1$ .

If the cross section is recorded on a db scale, the recorded quantity is  $10 \log f$ .

*It is assumed that the random variable,  $10 \log f$ , is normally distributed with mean  $m$  and variance  $A^2$ .* This assumption is not inconsistent with the observed data.

It is then a simple matter to obtain the following relationships:

$$m = -10 \log \langle f^2 \rangle = -\frac{\ln 10}{20} A^2 \sim -.115 A^2 .$$

These relationships enable one to find any two of the quantities,  $m$ ,  $A$ , or  $V_f$ , from the third.

On the basis of data received, both in the flight test and in the static inflation tests, typical values of  $A$  are 3 at the lower frequencies and 6 at the higher frequencies, giving corresponding values for  $m$  of -1 db and -3 db.

The cumulative probability distribution for  $f$  is

$$\phi\left(\frac{10 \log x - m}{A}\right) \quad x > 0$$

$$0 \quad x \leq 0 ,$$

where

$$\phi(u) = \frac{1}{\sqrt{2\pi}} \int_{-\infty}^u e^{-t^2/2} dt .$$

## Fading Rate

For a particular receiver sensitivity the minimal acceptable received power is specified. If the power and gain of the transmitting system, the effective aperture of the receiver antenna, and the trajectory of the Echo II are given, then by using the radar equation,

$$P_r = \frac{P_t G A_r}{16\pi^2 R_t^2 R_r^2} \sigma ,$$

this received power requirement can be translated into a minimal acceptable value of  $\sigma$  and  $\sigma_m$ . The value of  $\sigma_m$ , of course, varies depending on the variables  $R_t$  and  $R_r$ , and the respective distances from the balloon to the transmitter and receiver. For a particular value of  $\sigma_m$ , there is the probability that  $\sigma < \sigma_m$ , or equivalently, that  $f < \sigma_m/\sigma_0$ , which is

$$\phi \left( \frac{10 \log \frac{\sigma_m}{\sigma_0} + .115 A^2}{A} \right) < .01 , \quad \text{or}$$
$$- 10 \log \frac{\sigma_m}{\sigma_0} > .115 A^2 + 2.4A .$$

If  $A = 5$ ,  $\sigma_m$  must be 15 db below  $\sigma_0$ . When this value is inserted into the radar equation the minimal value of  $P_t$  can be determined. If  $A = 3$ ,  $\sigma_m$  need be only 6 db below  $\sigma_0$ . Therefore, going from  $A = 5$  to  $A = 3$  causes a 9 db reduction in the necessary transmitter power, for a fading rate  $< .01$ .

## Signal Modulation by the Balloon

Because the radar data determines the amplitude, but not the phase, of a reflected signal, discussion of balloon modulation has been limited to amplitude modulated signals.

The wave form of an amplitude modulated signal can be represented as

$$1 + s(t)$$

where  $s(t)$  is the modulation waveform which is the information carrying signal. If there is no further modulation by the transmission path, the waveform arriving at the receiver is unchanged and the detected waveform will be

$$s(t) + n(t) ,$$

where  $n(t)$  is the noise of the receiver system. This picture changes when the transmission path modulates the signal.

In particular, after reflection by the balloon, the waveform arriving at the receiver is

$$[1 + s(t)] \frac{\sigma(t)}{\sigma_0} = [1 + s(t)] \sqrt{f} .$$

The modulation waveform is therefore

$$s(t) \sqrt{f} + (\sqrt{f} - 1) = s(t) + [1 + s(t)] (\sqrt{f} - 1)$$

The detected signal is then

$$s(t) + [1 + s(t)] (\sqrt{f} - 1) + n(t) .$$

The term  $N(t) = [1 + s(t)] (\sqrt{f} - 1)$  is noise which has been added to the information carrying signal  $s(t)$ . If the signal ensemble is specified,  $s$  is a random variable. Then  $N(t)$  is a random variable whose distribution can be determined on the basis of the following:

If  $F$  and  $G$  are independent random variables with probability densities of  $D_F(x)$ ,  $D_G(x)$ , respectively, then the probability density for the random variable  $F, G$  is

$$D_{FG}(x) = \int_{-\infty}^{\infty} D_F(y) D_G\left(\frac{x}{y}\right) dy$$

Thus, since we have determined the distributed function for  $f$ , and hence for  $\sqrt{f} - 1$ , it is possible to find the distribution function for  $N$ . The average noise power is then the expected value

$$\langle N^2 \rangle = \langle (1 + s)^2 (\sqrt{f} - 1)^2 \rangle ,$$

and the signal to noise ratio

$$\frac{\langle S^2 \rangle}{\langle N^2 \rangle} ,$$

is the highest possible signal to noise ratio, even if the system noise is zero.

We have computed this ratio for two different signal ensembles as follows:

- (a)  $s$  is uniformly distributed over the range  $-P \leq x \leq P$ , where  $0 \leq P \leq 1$ , with  $P$  representing the modulation percentage. In this case

$$\frac{\langle S^2 \rangle}{\langle N^2 \rangle} = \frac{1}{16 A^2} \frac{P^2}{1 + P^2} \times 10^4$$

For  $A = 5$ , this ratio is approximately 12 for  $P = 1$  and 6 for  $P = 1/2$ .

For  $A = 3$ , this ratio is approximately 33 for  $P = 1$  and 16 for  $P = 1/2$ .

(b)  $s = 0$  and  $-1$  equal probability (keyed CW transmission). In this case,

$$\frac{\langle S^2 \rangle}{\langle N^2 \rangle} \sim \frac{3}{2} \frac{10^4}{A^2}$$

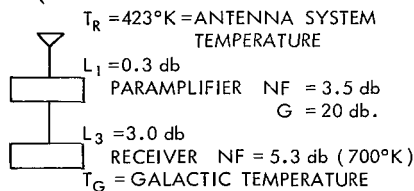
Here, even for  $A = 10$ , the ratio is 150.

## COMMUNICATIONS EXPERIMENT

An excellent opportunity to obtain large bistatic angle performance data at frequencies considerably lower than the 400 Mc radar of the original experiment, was afforded by the US-UK-

USSR experiments with the Echo II from 21 February to 8 March, 1964, conducted in accordance with an agreement between the USSR Academy of Sciences and NASA (USA), and representatives of the USSR Academy of Sciences, Gorkey State University and Jodrell Bank Observatory (UK).

ASSUMPTIONS: { JODRELL BANK TRANSMITS: 1KW, 162.4 Mc  
ZIMENKI RECEIVES



TOTAL SYSTEM TEMPERATURE  $T_S = T_R + T_G = 423^\circ\text{K} + 450^\circ\text{K}$   
 $T_S = 873^\circ\text{K}$

### SYSTEM PERFORMANCE

SPACE LOSS (2400 mi)	-245.3 db.
$P_t$ (1Kw)	30.0 dbw
$G_t$ (250')	39.5 db.
$G_r$ (45')	24.8 db.
CARRIER LEVEL	-151. dbw
<hr/>	
TOTAL SYSTEM NOISE $T_S$ (873°K)	29.42 db.
NOISE POWER DENSITY	-228.6 dbw/Mc.
NOISE POWER	-199.18 dbw/Mc.
<hr/>	
BANDWIDTH (1Kc)	30.0
NOISE LEVEL	-169.18 dbw IN 1 kc BANDWIDTH
<hr/>	
CARRIER/NOISE (1Kc) - 169.18 - 151 =	18.18 db
RECEIVER THRESHOLD 6 db	6.00 db
CARRIER/NOISE (1Kc)	12.18 db MARGIN

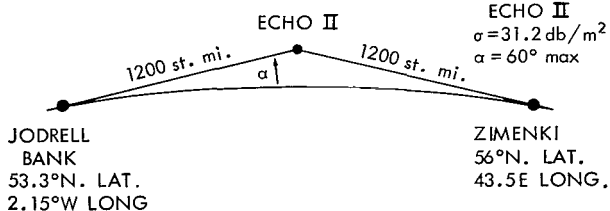


Figure 13—Jodrell bank—Zimunki data.

Calculations, prior to the experiment, Figure 13, indicate that an optimum pass occurring for a satellite with an orbit lying midway between Jodrell Bank and Zimunki, would yield a maximum carrier to noise level of 12.2 db for a 1 Kc bandwidth (this was nominally achieved during those passes for which maximum elevation angles were experienced for both stations). These computations included a 450°K noise contribution from galactic sources at 162.4 Mc.

Scintillations, however, varied from noise level as one limit, to levels of 10 db above those extrapolated from radar signature data at higher frequencies.

The recorded data for the Zimunki-Jodrell Bank tests are, unfortunately, not directly comparable to the monostatic, multi-frequency radar observations for rough

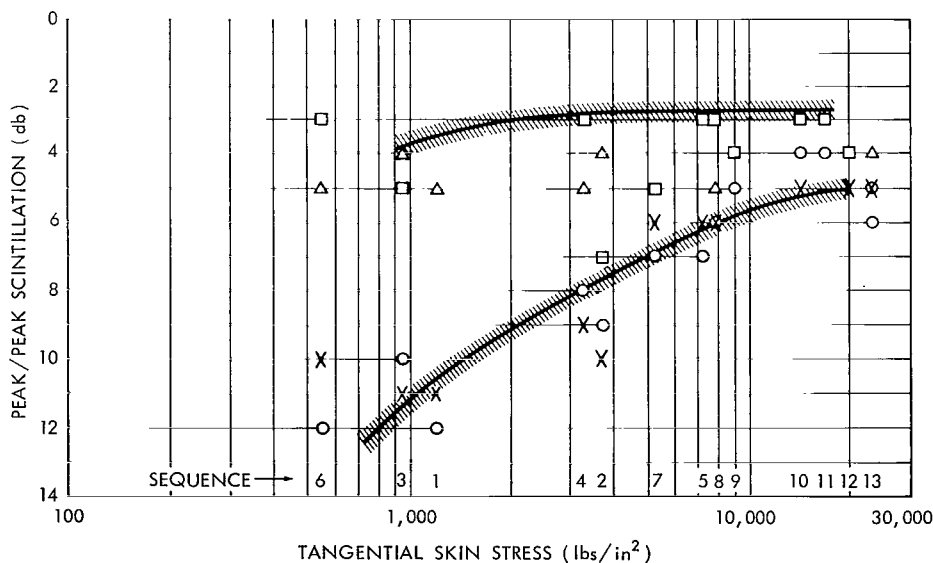
balloon surfaces. The experiment was characterized by multiple and cumulative degradations. Those characteristics of low elevation angle and multipath reception are most evident, since most passes provided receiving antenna look angles of 15 degrees or less. Faraday rotation was evident as depolarization of received signals (1600° rotation evident of 0° elevation to 80° rotation at 90° elevation), as well as cosmic noise variations (400°K to 1000°K at galactic center at 162 Mc. Further signal losses were attributed to antenna mispointing.\*

These tests do not obviate the necessity for continued investigation of passive communications satellites, nor attempts to provide such a nonfrequency sensitive communications medium which can accommodate equipment readily available, provided that sufficient signal margin is achieved to convey information.

### ADDITIONAL DATA

Figure 14 represents a series of measurements of a flight quality balloon inflated within the Naval Air Station hangar, Lakehurst, N. J. The data are plotted to show the sequence of measurements, from a minimum ambient pressure level (to yield a 600 psi skin stress), through intermediate skin stress levels, to an ultimate, maximum, skin stress of 20,000 psi. The resultant

\*A detailed NASA Technical Report on the USSR-UK-NASA Communications Experiment is in a final preparatory stage.



		PANELS		12-18-63 BALLOON # 16
		UNREINFORCED	REINFORCED	
C BAND		○	×	
L BAND		△	□	

Figure 14—Measurements on inflated balloon no. 16 at Lakehurst, New Jersey.

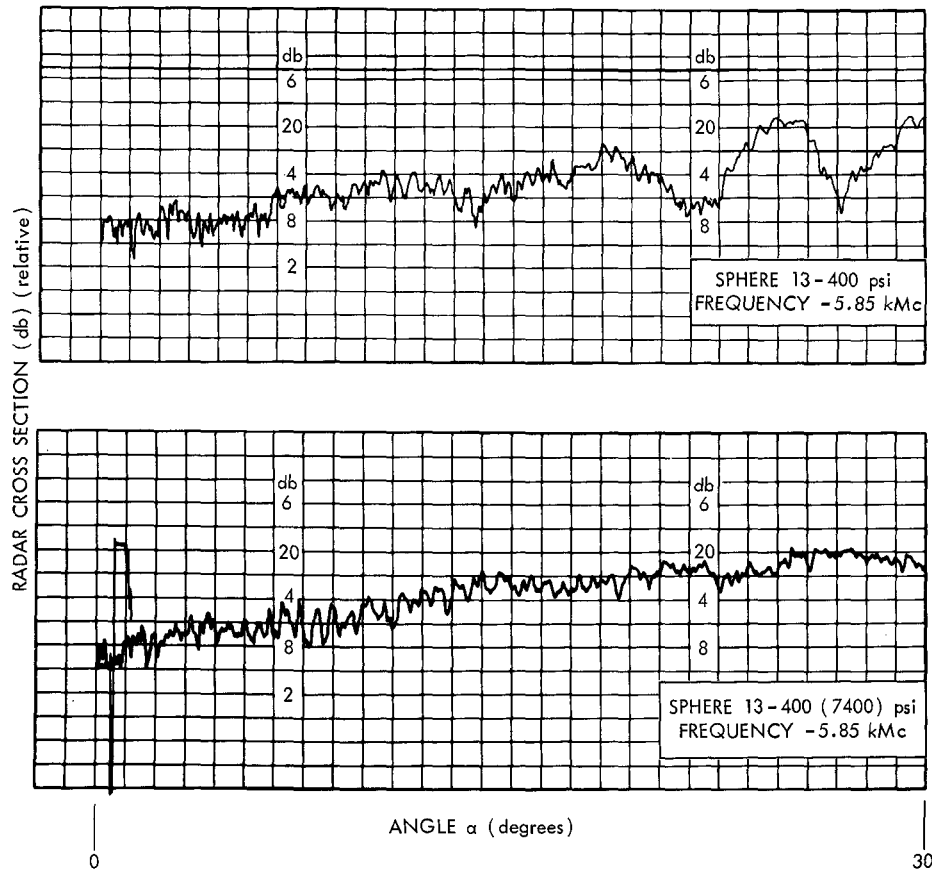


Figure 15—Direct recording of radar cross section versus the observation angle  $\alpha$  (Figure 5).

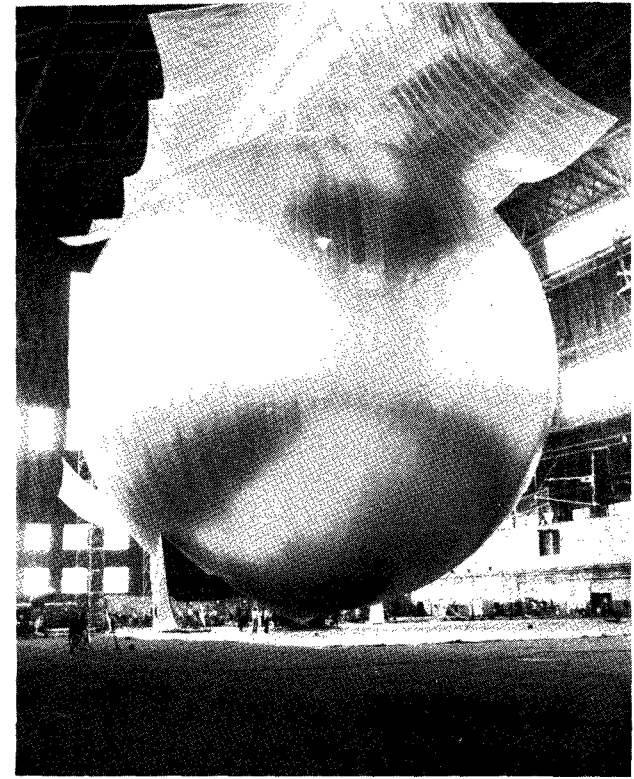


Figure 16—Close-up view of Echo II test sphere at Lakehurst, New Jersey.

peak-to-peak scintillation levels at L and C band frequencies reveal the asymptotic improvement of balloon behavior as a function of skin stresses.

Figure 15 is a reproduction of the recorded data of another flight quality balloon (no. 13) measured at the Lakehurst, New Jersey site.

Figure 16 is a photograph of Echo II showing a rupture of stressed skin (beyond 20,000 psi) which resulted in a cavernous hole. It is notable that this sphere, as shown, remained stationary for 45 minutes while radar data were recorded, and then slowly settled to the concrete pad.

(Manuscript received November 23, 1965)

#### REFERENCES

1. Weston, V. H., "Near-Zone Back-Scattering from Large Spheres," *Appl. Sci. Res. (Section B)*, 9:107-116 (1960).
2. Fock, V. A., "Generalization of the Reflection Formulas to the Case of an Arbitrary Wave from a Surface of Arbitrary Form," *Zh. Eksperim. i Teor. Fiz.*, 20:961-978, (1950).



## APPENDIX A

### Equations of Membrane Forces

The equations of equilibrium of a typical panel are:

$$N_{xx,x} + N_{xy,y} = 0 \quad (1)$$

$$N_{xy,x} + N_{yy,y} = 0 \quad (2)$$

$$N_{xx}w_{,xx} + 2N_{xy}w_{,xy} + N_{yy}w_{,yy} - \frac{N_{yy}}{R} = -p \quad (3)$$

In these equations, the first two constitute the condition of equilibrium in the tangent plane, and the third the one perpendicular to it. The membrane forces are  $N_{ij}$ , and the deflection perpendicular to the tangent plane is  $w$ . A comma, followed by a letter, constitutes partial differentiation with respect to the corresponding coordinate. Eqs. 1 to 3 are taken relative to the final configuration, although certain standard approximations inherent in shell theory have been made.

The equations relating the membrane forces to the membrane strains  $\epsilon_{ij}$  are as follows:

$$N_{xx} = K'(\epsilon_{xx} + \nu \epsilon_{yy}) \quad (4)$$

$$N_{yy} = K'(\epsilon_{yy} + \nu \epsilon_{xx}) \left( K' = \frac{ET}{1-\nu^2} \right) \quad (5)$$

$$N_{xy} = K'(1-\nu) \epsilon_{xy} \quad (6)$$

( $t$  = membrane thickness,  $E$  = Young's modulus,  $\nu$  = Poisson ratio.) Finally, the strain-displacement relations are given by

$$\epsilon_{xx} = u_{,x} + \frac{1}{2} w_{,x}^2 \quad (7)$$

$$\epsilon_{yy} = \nu_{,y} + \frac{1}{2} w_{,y}^2 + \frac{w}{R} \quad (8)$$

$$\epsilon_{xy} = \frac{1}{2} (u_{,y} + \nu_{,x} + w_{,x}w_{,y}) \quad (9)$$

in which  $u$  and  $v$  are, respectively, the displacements in the  $x$  and  $y$  directions. It is noted that non-linear terms in the lateral deflection  $w$  are retained.

The system of Eqs. 1 to 9 involves nine unknown variables: the three independent membrane forces  $N_{ij}$ ; the three displacement components  $u$ ,  $v$ , and  $w$ ; and the three independent membrane strain components  $\epsilon_{ij}$ . Eqs. 1 and 2 imply the existence of a stress function. Eqs. 7 to 9 imply a compatibility relation among the strains after the elimination of  $u$  and  $v$ . When this is substituted in Eqs. 3 to 6, there result two equations in the stress function and the deflection  $w$  (associated with the name of Foepl) which are of the sixth order.

The "boundary conditions" at the center of the panel are given by the symmetry conditions 10, 11, and 12 as follows:

$$N_{xy}(0, y) = 0 \quad (10)$$

$$w_{,x}(0, y) = 0 \quad (11)$$

$$u(0, y) = 0 \quad (12)$$

At the seam, the following two conditions

$$N_{xy}(\ell, y) = 0 \quad (13)$$

$$u(\ell, y) = w \tan \alpha \quad (14)$$

imply that, by symmetry, the shearing stress vanishes and the displacement is radial. A third condition can be obtained from conditions of equilibrium of the report;  $\ell$  represents half the width of the gore.

It is easily seen that the *linear* equations, (4), (5), and (6) are dimensionally invariant if  $K'$  and  $\nu$  do not change. However, because of the presence of the membrane thickness,  $t$  in the expression for  $K'$ , under scaling,  $E/1 - \nu^2$  must change by the inverse of the scale factor.

This similitude condition is supplemented by whatever scaling restrictions are implied by the non-linearity of the other equations.

## APPENDIX B

### Mathematical Model of the Balloon

Each panel of the balloon was assumed to have the equation

$$\vec{r} = \vec{r}(S_1, S_2),$$

where  $S_j, j = 1, 2$  are the arc lengths of the orthogonal coordinate curves. The full variation of  $S_1$  is the longitudinal perimeter of the gore, which is approximately  $\pi a$ ; for each  $S_1, S_2$  varies over the interval  $[-S/2, S/2]$ , in which  $S$ , of course, depends on  $S_1$ . The coordinate curves are plane curves, having the unit tangent vectors

$$\hat{T}_j(S_1, S_2) = \hat{t}_{s_j}(S_1, S_2), \quad j = 1, 2$$

and have curvatures  $K_j$ , which will be assumed to be constant and having the values  $1/a, 1/A$ , where  $A \geq a$ . The Frenet-Serret formulas are

$$\frac{\partial \hat{T}_j}{\partial S_j} = K_j \hat{n}, \quad \frac{\partial \hat{n}}{\partial S_j} = -K_j \hat{T}_j, \quad j = 1, 2$$

and

$$\hat{n} = \hat{T}_2 \times \hat{T}_1.$$

To complete the scattered field, it is assumed that the currents induced by the incident field are given by the Kirchoff approximation, valid for large  $a$ ,

$$= 2\vec{H}^{(i)} \times \hat{n},$$

where  $\vec{H}^{(i)}$  is the incident magnetic field. The transmitter will be assumed to be located in the direction of the unit vector  $\hat{u}_T$ , and the receiver in the direction of the unit vector  $\hat{u}_R$ . The bistatic angle,  $2\beta$ , is defined by

$$\cos 2\beta = \hat{u}_R \cdot \hat{u}_T,$$

and the unit vector  $\hat{u}_0$  is defined by

$$\hat{u}_0 = \frac{1}{2 \cos \beta} (\hat{u}_R + \hat{u}_T) .$$

The polarization of the incident field is given by the unit vector  $\hat{p}$ , where  $\hat{p} \cdot \hat{u}_T = 0$ . Then the scattered field  $\vec{H}^{(s)}$  is given by the Kirchoff formula. The normalized scattered field,  $\vec{H}$ , defined by

$$\vec{H} = \sqrt{4 \pi R^2} e^{-i k R} \vec{H}^{(s)} ,$$

is then, for large  $R$ , described by

$$\vec{H} = \frac{i k}{\sqrt{\pi}} \iint \exp(-2 i k \cos \beta \hat{u}_0 \cdot \vec{r}) (\hat{n} \times \hat{p}) \times \hat{u}_R dS ,$$

the integral being extended over the illuminated portion of the gore.

Because there is always a value of  $S_1$  for which  $\hat{u}_0 \cdot \vec{r}_{S_1} = 0$ , the above integral can be evaluated by regarding it as an iterated integral, and integrating, first with respect to  $S_1$  by the method of stationary phase (justified because  $ka$  is  $\gg 1$ ), we obtain

$$\vec{H} \sim i e^{\pi i / 4} \sqrt{\frac{ka}{\cos \beta}} \int_{-S/2}^{S/2} dS_2 \left\{ \frac{\exp[-2 i k \cos \beta \hat{u}_0 \cdot \vec{r}(S_1^*, S_2)]}{\sqrt{\hat{u}_0 \cdot \hat{n}(S_1^*, S_2)}} [\hat{n}(S_1^*, S_2) \times \hat{p}] \times \hat{u}_R \right\}$$

$S_1^*$  is the point for which  $\hat{u}_0 \cdot \vec{r}_{S_1}(S_1^*, S_2) = 0$ , and is independent of  $S_2$ ; hence, we can regard  $S_1^*$  as a constant in the evaluation of the integral.

The vector  $\hat{u}_0$  lies in the plane of the curve (because  $\hat{u} \cdot \hat{T}_2 = 0$ ), which is an arc of a circle with radius  $A$ . Let  $\alpha = \pi / 106 \sin \theta_0$ , where  $\theta_0$  is the azimuth angle of  $\hat{u}_0$ . [ $\theta_0 = \pi / 2$  corresponds to  $\hat{u}_0$  lying in the equatorial plane.], and

$$\frac{S}{2} = A \sin^{-1} \left( \frac{a}{A} \alpha \right) \sim a \alpha$$

Now, using the Frenet-Serret formulas, we obtain

$$\vec{r}(S_2) = \vec{r}(0) + \hat{T}_1(0) S_2 - \frac{1}{2A} \hat{n}(0) S_2^2 + \dots$$

$$\hat{n}(S_2) = \hat{n}(0) + \frac{\hat{T}_1(0)}{A} S_2 + \dots$$

It is clear that  $\hat{u}_0 \cdot \hat{n}(0) = \cos \psi_0$ ,  $\hat{u}_0 \cdot \hat{T}_1(0) = \sin \psi_0$ , and

$$\vec{r}(0) = \left[ a \cos \alpha + A \left( 1 - \cos \frac{a}{A} \alpha \right) \right] \hat{n}(0) \sim a \hat{n}(0) .$$

Therefore, the integral can be approximated as

$$\vec{H} \sim i e^{\pi i/4} \sqrt{\frac{ka}{\cos \beta}} \exp(-2ik a \cos \beta \cos \psi_0) \int_{-S/2}^{S/2} \frac{\exp \left[ i 2k \cos \beta \left( \frac{\cos \psi_0}{A} S_2^2 - 2 \sin \psi_0 S_2 \right) \right]}{\sqrt{\cos \psi_0 + \frac{S_2}{A} \sin \psi_0}} \left\{ \left[ \hat{n}(0) + \frac{\hat{T}_1(0)}{A} S_2 \right] \times \hat{p} \right\} \times \hat{u}_R dS_2$$

There are two independent orientations for the polarization vector  $\hat{p}$ . The first is perpendicular to the plane of the three vectors,  $\hat{u}_T$ ,  $\hat{u}_0$ ,  $\hat{u}_R$ , corresponding to horizontal electric polarization. For an arbitrary vector  $\hat{v}$ ,

$$[\hat{v} \times \hat{p}^{(1)}] \times \hat{u}_R = (\hat{u}_R \cdot \hat{v}) \hat{p}^{(1)} ,$$

where  $\hat{p}^{(1)}$  represents this polarization. In particular, if  $\hat{v} = \hat{n}(0)$  because  $\hat{u}_T$  lies on a cone of half-angle  $\beta$  about  $\hat{u}_0$ , then

$$\cos \beta \cos \psi_0 = \sin \beta \sin \psi_0 < (\hat{u}_R \cdot \hat{n}_0) < \cos \beta \cos \psi_0 \sin \beta \sin \psi_0$$

If  $0 \leq \beta \leq 15^\circ$  and  $0 \leq \psi_0 \leq 7-1/2^\circ$ , we may take

$$(\hat{u}_R \cdot \hat{n}_0) \sim \cos \beta \cos \psi_0 ,$$

so that the vector cross product term in the integrand can be replaced by

$$\cos \beta \cos \psi_0 \hat{p}_1 + 0 \left( \frac{S_2}{A} \right) .$$

The other orientation, corresponding to vertical electric polarization, is

$$\hat{p}^{(2)} = (\hat{u}_T \times \hat{p}^{(1)}) .$$

For arbitrary  $\hat{v}$ ,

$$\begin{aligned} (\hat{v} \times \hat{p}_2) \times \hat{u}_R &= [\hat{v} \times (\hat{u}_T \times \hat{p}^{(1)})] \times \hat{u}_R \\ &= [(\hat{v} \cdot \hat{p}^{(1)}) (\hat{u}_T \times \hat{u}_R) - (\hat{v} \cdot \hat{u}_T) (\hat{p}^{(1)} \times \hat{u}_R)] . \end{aligned}$$

The second vector corresponds to vertical electric polarization, whereas the first corresponds to  $\hat{u}_T \times \hat{u}_R = \sin 2\beta \hat{p}_1^{(1)}$ , a cross polarization term. If  $\hat{v} = \hat{n}(0)$ , as above  $(\hat{v} \cdot \hat{u}_T) \sim \cos \psi_0 \cos \beta$ , and since  $\hat{p}_1$  is orthogonal to  $\hat{u}_0$  and  $\hat{n}(0)$  makes an angle  $\psi_0$  with  $\hat{u}_0$ ,  $(\hat{v} \cdot \hat{p}^{(1)}) < |\sin \psi_0|$ .

With this approximation, the cross-product term in the integrand is

$$+ \cos \beta \cos \psi_0 (\hat{u}_R \times \hat{p}^{(1)}) + o\left(\frac{S_2}{A}\right) .$$

Now, neglecting terms  $o(S_2/A)$  in the slowly varying part of the integrand, and suppressing the polarization vector the factor  $ie^{\pi i/4}$ , we obtain

$$\vec{H} \sim \exp(-2ik a \cos \beta \cos \psi_0) \sqrt{ka \cos \beta \cos \psi_0} \int_{-S/2}^{S/2} \exp\left[ik \cos \beta \left(\frac{\cos \psi_0}{A} S_2^2 - 2 \sin \psi_0 S_2\right)\right] dS_2 .$$

For the values  $0 \leq \beta \leq 15^\circ$ ,  $0 \leq |\psi_0| \leq 7.5^\circ$ , a final approximation, and suppressing the constant phase term, we have

$$H \sim \sqrt{ka} \int_{-S/2}^{S/2} \exp\left[ik \left(\frac{S_2^2}{A} - 2\psi_0 \cdot S_2\right)\right] dS_2 .$$

Now, letting  $S/2 = a\xi$ ,  $\xi = S_2/a$ , and defining

$$y = \frac{A}{a} \quad (y \geq 1) ,$$

we obtain

$$\frac{\vec{H}}{\sqrt{\pi a^2}} \sim \frac{ka}{\pi} \int_{-a}^a \exp\left[ik a \left(\frac{\xi^2}{y} - 2\psi_0 \xi\right)\right] d\xi .$$

3/22/60  
02

*"The aeronautical and space activities of the United States shall be conducted so as to contribute . . . to the expansion of human knowledge of phenomena in the atmosphere and space. The Administration shall provide for the widest practicable and appropriate dissemination of information concerning its activities and the results thereof."*

—NATIONAL AERONAUTICS AND SPACE ACT OF 1958

## NASA SCIENTIFIC AND TECHNICAL PUBLICATIONS

**TECHNICAL REPORTS:** Scientific and technical information considered important, complete, and a lasting contribution to existing knowledge.

**TECHNICAL NOTES:** Information less broad in scope but nevertheless of importance as a contribution to existing knowledge.

**TECHNICAL MEMORANDUMS:** Information receiving limited distribution because of preliminary data, security classification, or other reasons.

**CONTRACTOR REPORTS:** Technical information generated in connection with a NASA contract or grant and released under NASA auspices.

**TECHNICAL TRANSLATIONS:** Information published in a foreign language considered to merit NASA distribution in English.

**TECHNICAL REPRINTS:** Information derived from NASA activities and initially published in the form of journal articles.

**SPECIAL PUBLICATIONS:** Information derived from or of value to NASA activities but not necessarily reporting the results of individual NASA-programmed scientific efforts. Publications include conference proceedings, monographs, data compilations, handbooks, sourcebooks, and special bibliographies.

*Details on the availability of these publications may be obtained from:*

SCIENTIFIC AND TECHNICAL INFORMATION DIVISION  
NATIONAL AERONAUTICS AND SPACE ADMINISTRATION

Washington, D.C. 20546